Korean J. Chem. Eng., **31**(2), 322-326 (2014)
DOI: 10.1007/s11814-013-0230-5

pISSN: 0256-1115
eISSN: 1975-7220

Direct synthesis of bi-modal porous structure MCM-41 and its application in CO_2 capturing through amine-grafting

Mohsen Gholami†, Mohammad Reza Talaie, and Seyed Foad Aghamiri

Department of Chemical Engineering, College of Engineering, University of Isfahan, P. O. Box 81746-73441, Isfahan, Iran
(*Received 9 August 2013 • accepted 27 October 2013*)

Abstract−A bi-modal porous structure MCM-41 (BPS-MCM-41) was synthesized and functionalized by 3-[2-(2-Aminoethylamino)ethylamino]propyltrimethoxysilane (TRI); also, its performance in amine grafting and CO_2 capturing was compared with that of pore-expanded MCM-41 [1]. To create larger pores beside the mesoporous structure of MCM-41, carbon black nanoparticles were used as the solid template. Characterizing the BPS-MCM-41 using the BET and BJH techniques resulted in the surface reduction of 29.3 percent and volume increase of 68.46 percent. The pore size distribution showed two peaks: a narrow peak at 2.24 nm diameter, which belonged to micelles, and a wide one at about 50 nm due to the presence of used nanoparticles. The functionalization confirmed that BPS-MCM-41 is capable of accommodating a large quantity of amine groups. The CO_2 adsorption measurement indicated that internal volume of the adsorbent was a critical factor affecting the adsorption capacity of the amine grafted adsorbents.

Keywords: Amine Grafted Adsorbent, BPS-MCM-41, CO_2 Capture, Hierarchical Structure, Amine Loading

INTRODUCTION

CO_2 removal from a gas stream has been the subject of many researches for a long time. CO_2 removal has been done because of industrial problems such as CO_2 freeze out in a demethanizer tower or to prevent corrosion and improve product quality in a natural gas refinery [2]. However, in the past two decades, the greenhouse effect has been the concern of many researchers in CO_2 capture [3]. To ease such a concern, researchers have begun to think of various ways, one of which is adsorption. Because of simplicity and flexibility of operation, adsorption is a promising method for capturing CO_2 [4].

Although CO_2 capture by adsorption from a humid gas has recently intrigued researchers due to the above-mentioned characteristics, the first studies conducted in this field date back to 1974 [5]. Many researches have shown that it is feasible to first remove the water and then capture the CO_2 by applying industrial adsorbents such as A and X type zeolites, but it makes the whole process uneconomical. This reason has made the physisorption impotent [6-15]. In 1994, Hogendoorn et al. [16] showed that by impregnating amine groups into solid particles, it is possible to use the benefits of chemical absorption and adsorption. However, only limited amounts of amine groups can be loaded because of the nature of the support material.

In 1992, by developing the M41S family, because of their high surface area and internal volume and tunable pore size, a new prospect was introduced into the field of CO_2 adsorption on functionalized adsorbents [17]. Amine loading, uniform distribution of functional groups, and mass transfer inside the particles are directly related to surface area, internal volume, and pore diameter of the support. Therefore, many researchers have focused on the functionalization of amine groups inside pore-enlarged adsorbents [18-23]. Although pore expansion increased the amine loading and CO_2 adsorption capacity, the ratio of solid particle diameter to pore diameter is still large. Mesoporous particles are of micrometric scale, and expanded pore diameter is about 15 nm. This shows that the ratio of mass transfer length (particle size) to pore diameter is more than 60. Thus, it is possible that agglomeration of functional groups in pore mouth might have caused blockage inside the particle.

One way which has been recently used to dispose of this limitation and also to enhance mass transfer rate is the development of hierarchical structures [24-29]. The logic behind this method is to create some larger pathways which cause less hindrance to mass transfer deep inside the particles, instead of expanding all pores [27]. This hierarchization is typically done by hard casting method, which involves a colloidal particle dispersion in synthesis gel; later, in the calcination step these particles are removed and their vacant places play the role of macrometric pathways [28].

As mentioned, uniform distribution of functional groups in the support material and the amine loading itself are of key parameters in CO_2 adsorption capacity. Functionalization of pore-expanded mesoporous materials such as pore-expanded MCM-41 (PE-MCM-41) by amine functional groups like TRI, has been investigated and well optimized by many researchers [1,30-36]. But functionalization of hierarchical mesoporous material is still immature [26,37]. Therefore, our aim was to synthesize a bi-modal porous structure MCM-41 (BPS-MCM-41) and to functionalize it with TRI in order to examine the amine loading and CO_2 adsorption capacity of amine grafted BPS-MCM-41.

MATERIALS

The chemical reagents used to synthesize and functionalize the BPS-MCM-41 are Cetyltrimethylammonium bromide (CTAB,

†To whom correspondence should be addressed.
E-mail: MGholami_ui@yahoo.com

Merck), deionized water, NH_4OH (25%, Merck), TEOS (Merck), carbon black nanoparticle (YongFeng, average particle size: 29 nm, surface area 118 m^2/gr), toluene (Merck), 3-[2-(2-Aminoethylamino) ethylamino]propyltrimethoxysilane (TRI, Sigma-Aldrich), and normal pentane (Merck), 5A zeolite (ZeoChem).

The gases used in this study were purchased from Farafan Gas Company. The specification of the gases is as follows: Carbon dioxide (high purity grade, 99.995%) and nitrogen (high purity grade, 99.995%).

EXPERIMENTAL PROCEDURE

1. Bi-modal MCM-41 Synthesis and TRI Grafting

The standard MCM-41 silica was prepared according to the standard procedure in the literature [17,38-40]. Typically, 4.88 gr of CTAB was dissolved in 202.5 gr of deionized water. After attaining a clear solution, 22.73 cc of NH_4OH (25%) was added and stirred for 10 minutes, then 20 cc of TEOS was added dropwise in 30 minutes to reach CTAB: 0.15, H_2O: 126, NH_4OH: 1.64 and TEOS: 1 molar ratios. The solution was then sealed and stirred for 3 hours in ambient temperature. Finally, it was put in an oven at 100 °C for 48 hours. The final product was filtered and washed with deionized water and dried at 80 °C overnight. Calcination was performed through a one-degree per minute temperature rise up to 550 °C, and after reaching 550 °C the status quo was maintained for five hours.

The procedure and reagents to hierarchize MCM-41 structure are the same as the ones in standard MCM-41; the hierarchizing material is the only difference between these two cases. In this study, carbon black nanoparticle was used as the solid template to create larger pores. After dissolving CTAB, Carbon black powder, which had already been degased at 200 °C for 2 hours, was added to the solution and mixed by ultrasonic homogenizer (Sonopuls HD2200 Sonicator, Bandelin) for 30 minutes at five cycles and 35% power. Then the synthesis procedure went on as it did with standard MCM-41. Note that to extract the carbon black from the silica structure, the calcination was performed under air flow.

Amine grafting was performed with the procedure of Guerrero et al. [36]. Typically, 1 gr of BPS-MCM-41 was dispersed in 75 ml of toluene. Prior to using toluene, it was dried using 5A zeolite. After 30-minutes vigorous mixing, 0.3 cc of deionized water was added to the mixture and was mixed for three hours. Then the glass flask was submerged in silicon oil bath at 85 °C and subsequently 3 cc of TRI was added under stirring and held under full reflux for 16 hours. The material was next filtered and washed with copious amount of toluene, followed by normal pentane. Finally, the filtered solid was dried at 80 °C in a circulating oven for one hour. Then, it was heated to 200 °C and held for one hour under nitrogen flow to remove dangling methoxy ligands.

2. Characterization

The structural properties of MCM-41 and BPS-MCM-41 were determined by XRD (X-ray Diffractometer, D8ADVANCE, Bruker, Germany, X-Ray Tube Anode: Cu Wavelength: 1.5406 Å (Cu Kα), Filter: Ni), and nitrogen adsorption/desorption at 77 K (BELsorp-mini II). The surface area was determined by the BET method, and pore size distribution was calculated by BJH method. Pore volume was calculated based on the amount of liquid nitrogen adsorbed at P/P_0=0.995 and simple density measurement. The CHNS elemental analyzer (LECO 932) is used to measure the amount of TRI grafted inside the BPS-MCM-41. Before the CHNS test, the adsorbent was degased under 0.01 bar absolute pressure at 100 °C to remove any adsorbed material. The CHNS test provides the mass percent of elemental carbon, hydrogen, nitrogen, and sulfur in adsorbent. Then, the mass fraction of elemental nitrogen was converted to moles of elemental nitrogen per unit mass of adsorbent by dividing the mass fraction by molecular weight of elemental nitrogen.

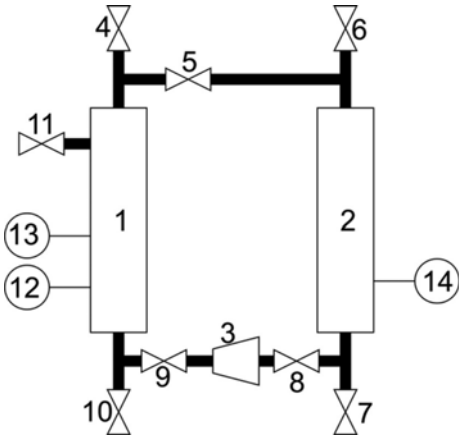

Fig. 1. Schematic diagram of closed loop volumetric apparatus.

1. Loading cell	11. Needle valve
2. Adsorption cell	12. RH and temperature sensor
3. Circulating pump	13. Pressure transmitter
4-10. Ball valve	14. RTD temperature sensor

3. CO_2 Adsorption Experiment

To measure equilibrium of CO_2 adsorption on synthesized adsorbent, a simple but robust closed-loop volumetric apparatus was developed (Fig. 1). The idea of developing such an apparatus was adopted from research done by Wang an LeVan [41]. The system consists of two cells (loading and adsorption cell), a variable-speed circulating pump, a pressure transmitter, an RTD temperature sensor and an RH sensor.

To measure the equilibrium adsorption data of CO_2 on the amine grafted BPS-MCM-41, first the adsorbent was degased under 0.01 bar absolute pressure at 100 °C. Then, a measured amount of the adsorbent was loaded into the adsorption cell under N_2 atmosphere. Before loading the adsorbent the whole volume of the setup was purged by N_2. During loading the adsorbent and purging by N_2, the valves 4, 5, 8 and 9 were open and the rest were closed. After loading, valve 4 was closed and pressure was increased to 1 bar gauge. Then valves 5 and 9 were closed and the loading cell was filled by definite amounts of N_2 and CO_2 with total pressure the same as the pressure of adsorption cell. After preparing the adsorbing gas in loading cell, valves 5 and 9 were opened and the circulating pump was turned on. Due to the adsorption of CO_2, the pressure changed, and the amount of the adsorbed CO_2 was calculated based on the total pressure change after enough time.

RESULTS AND DISCUSSION

1. Characterization of Standard and BPS-MCM-41

The XRD patterns of standard MCM-41 and BPS-MCM-41 are shown in Fig. 2. This figure shows less intensity as the C/CTAB

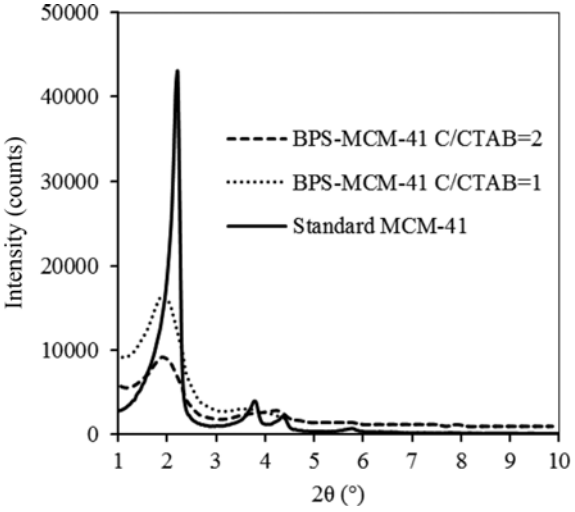

Fig. 2. The XRD pattern of Standard MCM-41 and BPS-MCM-41.

ratio increases. This trend indicates that as the C/CTAB increases, the structural order decreases. However, the angle at which the major peak (first peak) occurs is almost the same for all cases. This indicates that although the structural order has decreased due to the presence of carbon black, there are some pores with the same diameter in all three cases. The structural properties of MCM-41 and BPS-MCM-41 determined by nitrogen adsorption and density measurement are shown in Table 1. As the C/CTAB increases, the pore volume increases, but the surface area decreases. This indicates that the presence of carbon black nanoparticles causes condensation of TEOS on the surface of carbon nanoparticles which are covered by CTAB molecules. However, the presence of these carbon nanoparticles decreases the structural order, which results in the reduction of surface area.

Fig. 3(a)-(c) show the N_2 adsorption desorption curves at 77 K. As shown, for Standard MCM-41 at relative pressure of about 0.35, there is a steep rise in adsorbed volume due to capillary condensation in micellar pores. For the cases of BPS-MCM-41, after the rise at the relative pressure of 0.35, there is another rise at the relative pressure of about 0.9 due to capillary condensation in larger pores. The hysteresis between adsorption and desorption for both cases of BPS-MCM-41 shows that there is distribution in pore size, which is well justified in Fig. 4.

Fig. 5 and Fig. 6 show cumulative volume and cumulative surface area distribution, respectively. As shown in Fig. 5, as the C/CTAB ratio increases, cumulative volume distribution shows a higher value in larger pores. From Fig. 6, although total surface area decreases as C/CTAB ratio increases, it has a higher value at larger pore size.

2. Amine Loading and CO_2 Adsorption

Table 2 summarizes the amine loading of amine grafted BPS-MCM-41 and PE-MCM-41. As shown, although the surface area and pore volume of PE-MCM-41 are higher than those of BPS-MCM-41, the amount of amine loading is almost the same. However, due to having smaller surface area and pore volume, the surface density and volume density of amine groups are higher for BPS-MCM-41. It demonstrates that the presence of macropores beside mesopores makes the functionalization performance of BPS-MCM-41 better than the one of PE-MCM-41.

The CO_2 adsorption performance of amine grafted BPS-MCM-41 and that of amine grafted PE-MCM-41 are compared in Table 3. Although the total pressures for the cases are different, the CO_2 partial pressure and temperature, which are the key factors in thermodynamic equilibrium at low pressure, are the same. The adsorption capacity and amine group adsorption efficiency of PE-MCM-41 are higher than those of BPS-MCM-41. It is because of higher surface area and internal volume of the PE-MCM-41. However, when it comes to comparing the surface density and volume density of adsorbed CO_2, the results are almost the same. This fact confirms the important role of macroporous structure besides mesoporous structure.

Also, BPS-MCM-41 functionalization is done at the optimum point which Harlick and Sayari [31] obtained to functionalize PE-MCM-41. This optimum point is not necessarily the optimum point for BPS-MCM-41, but this condition was applied in BPS-func-

Table 1. The structural properties of MCM-41 and BPS-MCM-41

	MCM-41	BPS-MCM-41	BPS-MCM-41
Carbon black/CTAB (gr/gr)	0	1	2
a_s (BET) (m^2/gr)	1028	808.35	726.48
Total pore volume (cm^3/gr)	0.872	1.176	1.469
Mean pore diameter (nm)	3.394	5.817	8.089
a_p (BJH plot) (m^2/gr)	1222.3	924.6	678.3
v_p (BJH plot) (cm^3/gr)	0.804	1.081	1.386
r_{peak} (BJH plot) (nm)	1.22	1.22	1.22
V_{meso} (cm^3/gr)	0.7914	0.946	1.056
V_{macro} (cm^3/gr)	0.0134	0.190	0.330
a_{meso} (m^2/gr)	1221.564	916.784	659.202
a_{macro} (m^2/gr)	0.7356	12.08	19.098
Surface reduction %	0	21.4	29.3
Volume increase (BET) %	0	36.00	68.46
Bulk density (gr/cm^3)	0.199	0.173	0.148
Volume increase (density measurement) (cm^3/gr)	0	0.755	1.74

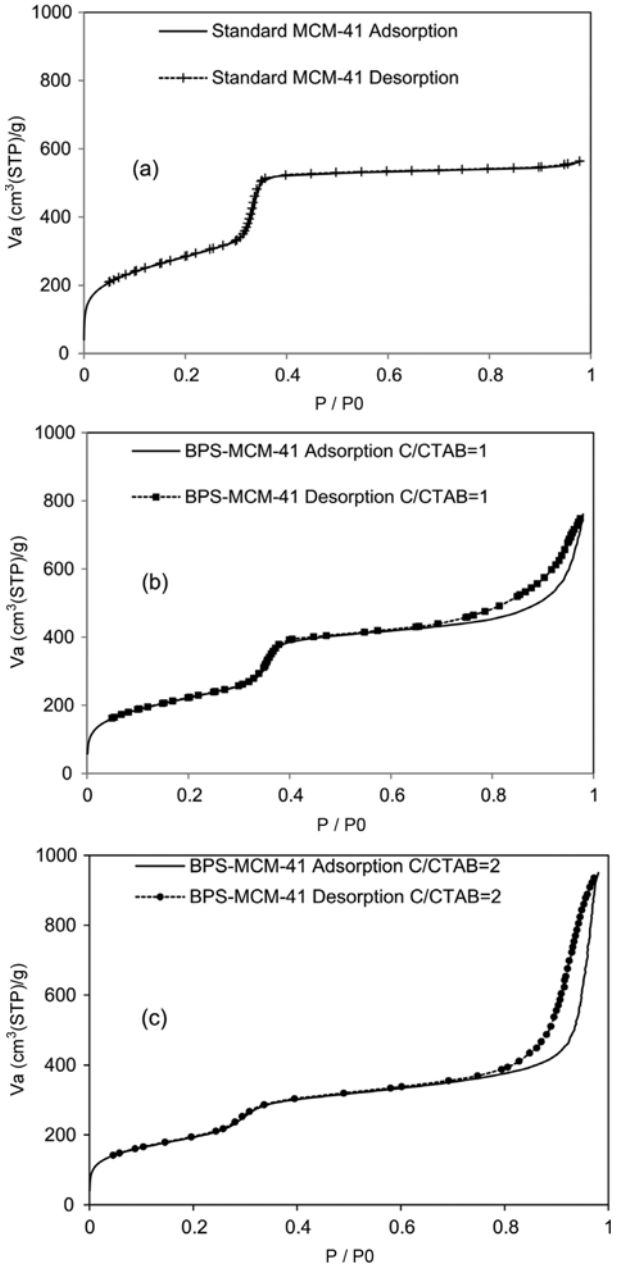

Fig. 3. N_2 adsorption desorption curve at 77 K, (a) standard MCM-41, (b) BPS-MCM-41 C/CTAB=1, (c) BPS-MCM-41 C/CTAB=2.

tionalization to have an objective comparison between them.

CONCLUSION

Carbon black nanoparticles were used to create BPS-MCM-41. The results showed that by using carbon black nanoparticles, hierarchical pore size distribution was created besides mesoporous structure of MCM-41. Due to hierarchization, the surface area was reduced by 29.3 percent, but the internal volume was increased by 68.46 percent. The pore size distribution results showed the presence of pores with diameter larger than 50 nm.

The amine grafting results showed that almost the same amount of functional groups could be loaded in BPS-MCM-41 with surface area and internal volume both smaller than those of PE-MCM-41. It showed a better functionalization performance.

The results of CO_2 adsorption measurement showed that although mass capacity of amine grafted PE-MCM-41 is higher than the capacity of amine grafted BPS-MCM-41, their volumetric capacities are almost the same. This fact confirms the important role of macroporous structure besides mesoporous structure. Also noteworthy is that the internal volume of the adsorbent is a critical factor affecting the adsorption capacity of the amine grafted adsorbents.

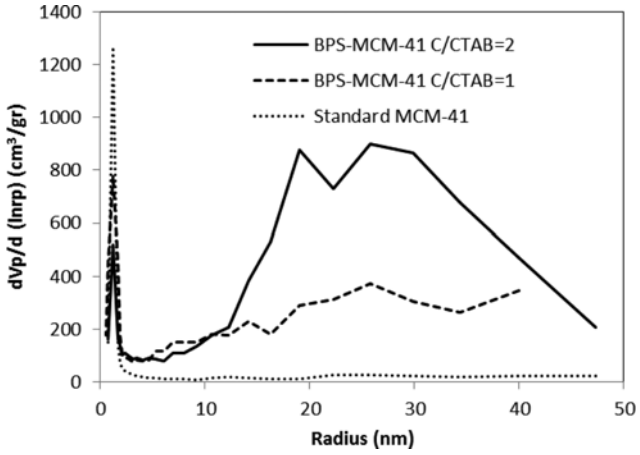

Fig. 4. Pore size distribution of standard MCM-41 and BPS-MCM-41.

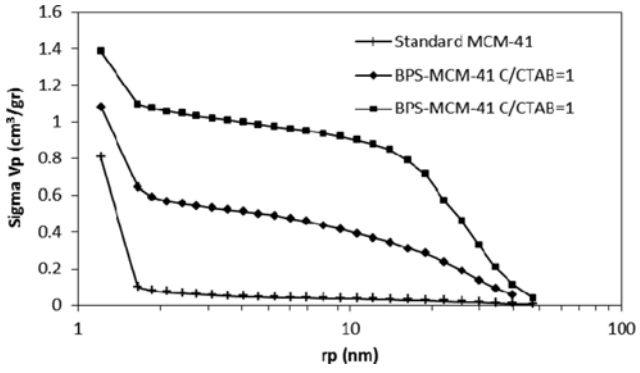

Fig. 5. Cumulative volume distribution.

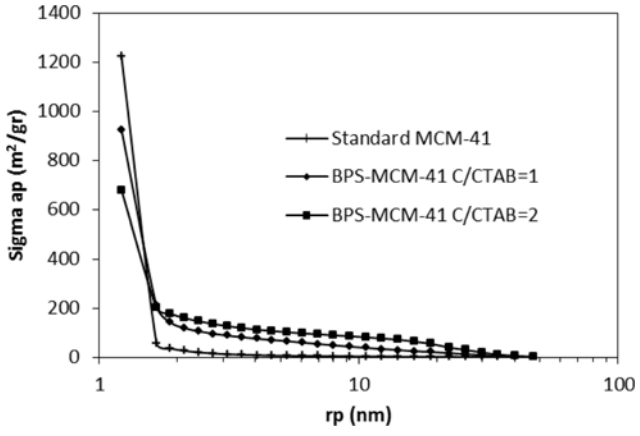

Fig. 6. Cumulative surface area.

Table 2. Comparison of amine loading on BPS-MCM-41 and PE-MCM-41

Support material	Surface area (m^2/gr)	Pore volume (cm^3/gr)	N (mmol/gr)	N (ìmol/m^2)	N (mmol/cm^3)	Reference
BPS-MCM-41	678.3	1.469	7.56 (CHNS)	11.15	5.15	Present study
PE-MCM-41	950	2.21	7.98 (TGA)	8.4	3.61	[31]

Table 3. Comparison of CO_2 adsorption performance on amine-grafted BPS-MCM-41 and PE-MCM-41

Support material	CO_2 partial pressure (kPa) balanced with N_2	Total absolute pressure (bar)	Dry CO_2 adsorption capacity at 298 K (mmol/gr)	CO_2/N ratio	CO_2/N ratio/m^2 *1000	CO_2/N ratio/cm^3	CO_2/m^2 (μmol/m^2)	CO_2/cm^3 (mmol/cm^3)	Reference
BPS-MCM-41	5	1.82	1.74	0.23	0.34	0.157	2.57	1.18	Present study
PE-MCM-41	5	1.00	2.65	0.332	0.35	0.15	2.79	1.19	[31]

ACKNOWLEDGEMENT

The authors would like to thank NIGC for financial support.

REFERENCES

1. P. J. E. Harlick and A. Sayari, *Ind. Eng. Chem. Res.*, **45**, 3248 (2006).
2. A. L. Kohl and R. B. Nielsen, *in* "Gas Purification (Fifth Edition)", Gulf Professional Publishing, Houston, 40 (1997).
3. A. Meisen and X. Shuai, *Energy Convers. Manage.*, **38, Supplement**, S37 (1997).
4. S. Choi, J. H. Drese and C. W. Jones, *ChemSusChem*, **2**, 796 (2009).
5. J. W. Carter and H. Husain, *Chem. Eng. Sci.*, **29**, 267 (1974).
6. C. M. Shen and W. M. Worek, *Int. J. Heat Mass Transfer*, **37**, 2123 (1994).
7. H. Mohamadinejad, J. C. Knox and J. E. Smith, *Sep. Sci. Technol.*, **35**, 1 (2000).
8. S. U. Rege, R. T. Yang, K. Qian and M. A. Buzanowski, *Chem. Eng. Sci.*, **56**, 2745 (2001).
9. N. Konduru, P. Lindner and N. M. Assaf-Anid, *AIChE J.*, **53**, 3137 (2007).
10. G. Li, P. Xiao, P. Webley, J. Zhang, R. Singh and M. Marshall, *Adsorption*, **14**, 415 (2008).
11. Y. Wang and M. D. LeVan, *J. Chem. Eng. Data*, **55**, 3189 (2009).
12. G. Li, P. Xiao, P. A. Webley, J. Zhang and R. Singh, *Energy Procedia*, **1**, 1123 (2009).
13. G. Li, P. Xiao and P. Webley, *Langmuir*, **25**, 10666 (2009).
14. N. Tlili, G. Grevillot and C. Vallieres, *Int. J. Greenhouse Gas Control*, **3**, 519 (2009).
15. Y. Wang and M. D. LeVan, *J. Chem. Eng. Data*, **55**, 3189 (2010).
16. J. A. Hogendoorn, W. P. M. Van Swaaij and G. F. Versteeg, *Chem. Eng. Sci.*, **49**, 3421 (1994).
17. J. S. Beck, J. C. Vartuli, W. J. Roth, M. E. Leonowicz, C. T. Kresge, K. D. Schmitt, C. T. W. Chu, D. H. Olson and E. W. Sheppard, *J. Am. Chem. Soc.*, **114**, 10834 (1992).
18. D. D. Das, P. J. E. Harlick and A. Sayari, *Catal. Commun.*, **8**, 829 (2007).
19. S. Loganathan, M. Tikmani and A. K. Ghoshal, *Langmuir*, **29**, 3491 (2013).
20. S. Jana, A. Mochizuki and S. Namba, *Catal. Surv. Asia*, **8**, 1 (2004).
21. M. Horňáček, P. Hudec and A. Smiešková, *Chem. Pap.*, **63**, 689 (2009).
22. A. Kierys, W. Buda and J. Goworek, *J. Porous Mater.*, **17**, 669 (2010).
23. M. Mizutani, Y. Yamada and K. Yano, *Chem. Commun.*, 1172 (2007).
24. A. Stein, *Micropor. Mesopor. Mater.*, **44-45**, 227 (2001).
25. C. Danumah, S. Vaudreuil, L. Bonneviot, M. Bousmina, S. Giasson and S. Kaliaguine, *Micropor. Mesopor. Mater.*, **44-45**, 241 (2001).
26. C. Chen, S.-T. Yang, W.-S. Ahn and R. Ryoo, *Chem. Commun.*, 3627 (2009).
27. J. Du, X. Lai, N. Yang, J. Zhai, D. Kisailus, F. Su, D. Wang and L. Jiang, *ACS Nano*, **5**, 590 (2011).
28. X.-Y. Yang, Y. Li, A. Lemaire, J.-G. Yu and B.-L. Su, *Pure Appl. Chem.*, **81**, 2265 (2009).
29. Q. Lei, T. Zhao, F. Li, Y. Wang and L. Hou, *J. Porous Mater.*, **15**, 643 (2008).
30. R. S. Franchi, P. J. E. Harlick and A. Sayari, *Ind. Eng. Chem. Res.*, **44**, 8007 (2005).
31. P. J. E. Harlick and A. Sayari, *Ind. Eng. Chem. Res.*, **46**, 446 (2006).
32. Y. Belmabkhout and A. Sayari, *Adsorption*, **15**, 318 (2009).
33. R. Franchi, P. J. E. Harlick, A. Sayari, S. Abdelhamid and J. Mietek, *in* "Studies in Surface Science and Catalysis", Elsevier, **156**, 879 (2005).
34. R. Serna-Guerrero, Y. Belmabkhout and A. Sayari, *Chem. Eng. Sci.*, **65**, 4166 (2010).
35. A. Heydari-Gorji, Y. Belmabkhout and A. Sayari, *Langmuir*, **27**, 12411 (2010).
36. R. Serna-Guerrero, Y. Belmabkhout and A. Sayari, *Adsorption*, **16**, 567 (2010).
37. G. Qi, Y. Wang, L. Estevez, X. Duan, N. Anako, A.-H. A. Park, W. Li, C. W. Jones and E. P. Giannelis, *Energy Environ. Sci.*, **4**, 444 (2011).
38. D. Kumar, K. Schumacher, C. du Fresne von Hohenesche, M. Grun and K. K. Unger, *Colloids Surf., A*, **187-188**, 109 (2001).
39. X. Xu, C. Song, J. M. Andrsen, B. G. Miller and A. W. Scaroni, *Micropor. Mesopor. Mater.*, **62**, 29 (2003).
40. J. C. Vartuli, W. J. Roth, J. S. Beck, S. B. McCullen and C. T. Kresge, *in* "Synthesis", Springer Berlin Heidelberg, **1**, 97 (1998).
41. W. Yu and M.D. LeVan, *J. Chem. Eng. Data*, **54**, 2839 (2009).